Supplementary Information

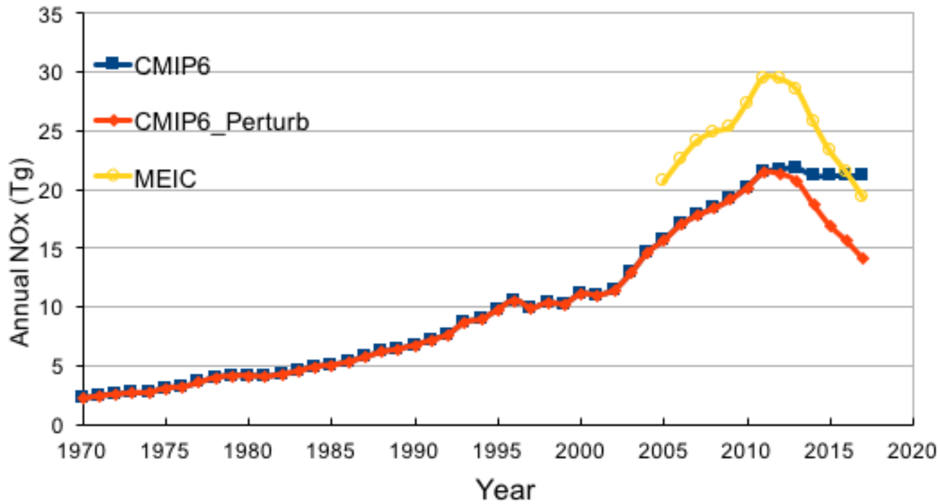

Figure S1. NO_X emission trends over China as estimated in the CMIP6 inventory (blue) and in MEIC (Multi-resolution Emission Inventory for China, yellow). The red line shows adjusted NO_X emissions used in this study.

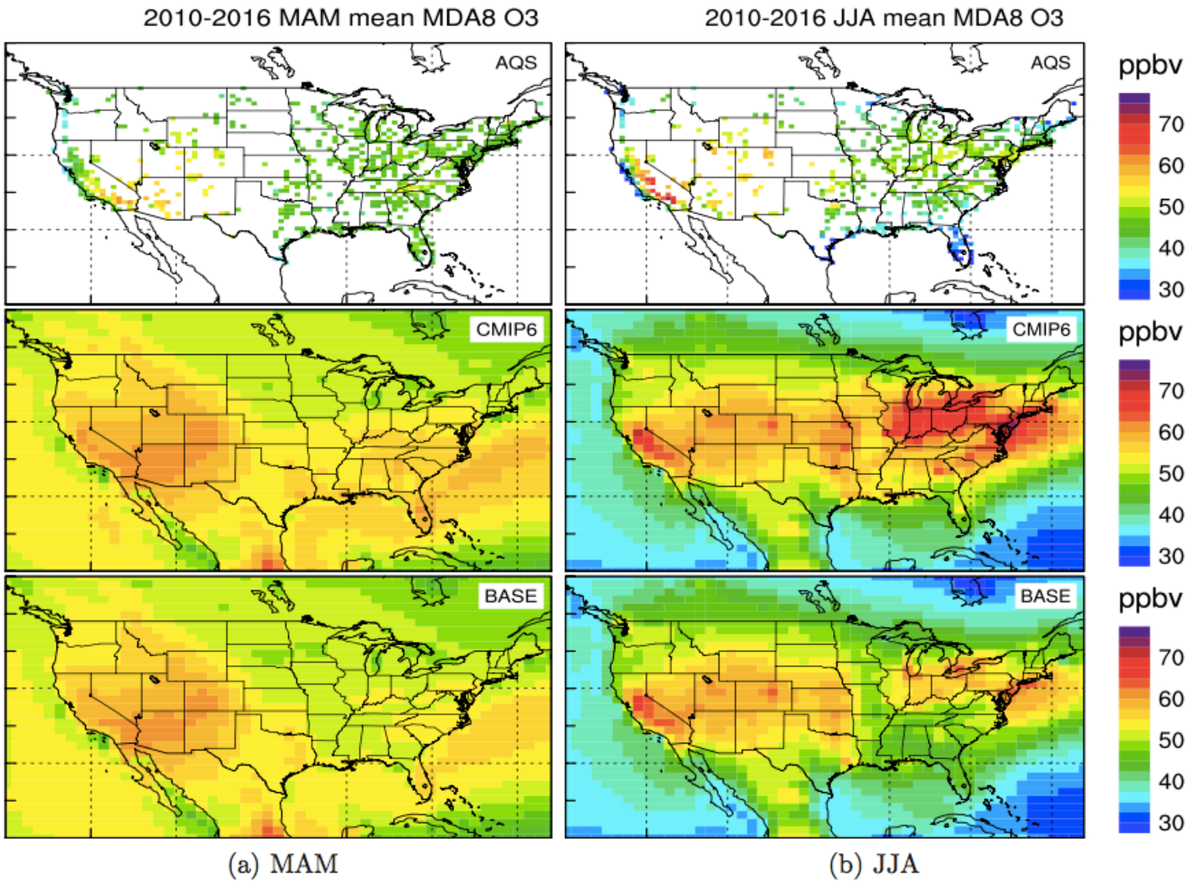

Figure S2. Spring (MAM) and summertime (JJA) mean MDA8 O_3 over the continental U.S. during 2010-2016 from AQS observations (top panels), GFDL-AM4 simulations with original CMIP6 emissions (middle panels) and adjusted emissions over the U.S. and China as described in the text (bottom panels) Observations at AQS sites are gridded into 0.5° × 0.625°.

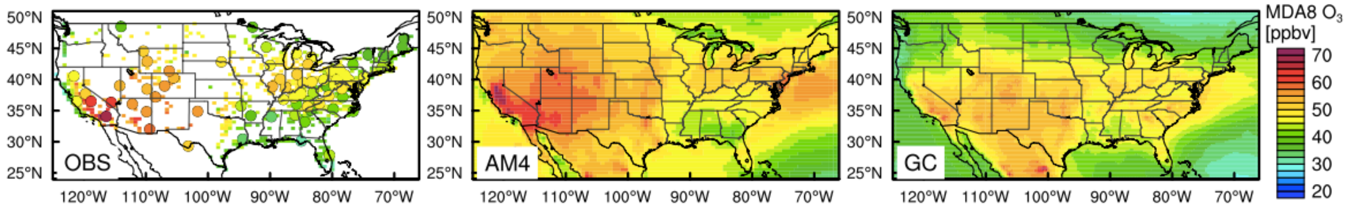

Figure S3. Spatial distributions of mean MDA8 O_3 during FAST-LVOS (May-June, 2017) as observed (OBS) and simulated with GFDL-AM4 (AM4) and GEOS-Chem (GC). Squares denote the AQS sites over 0.5° × 0.625° grids and circles the CASTNet sites.

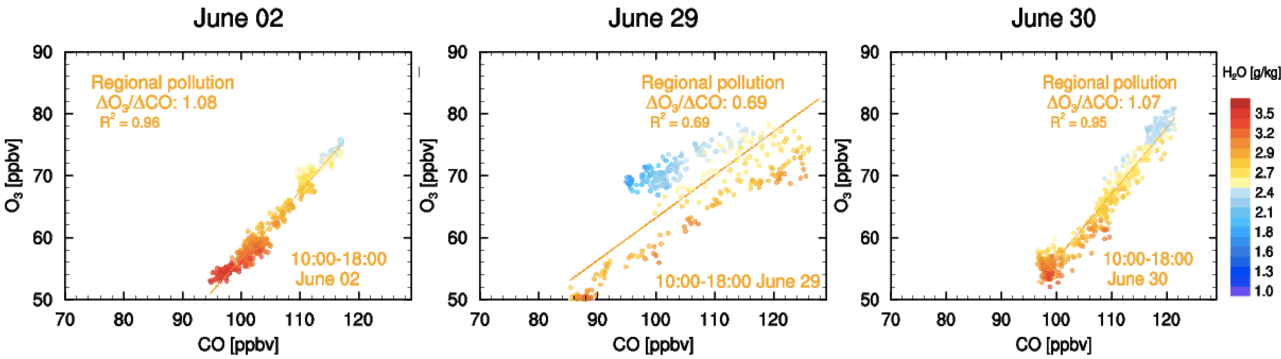

Figure S4. Scatter plots of 1-min O_3 against CO measured at Angel Peak, color-coded by specific humidity, for air masses influenced by regional pollution on June 02, June 29, and June 30.

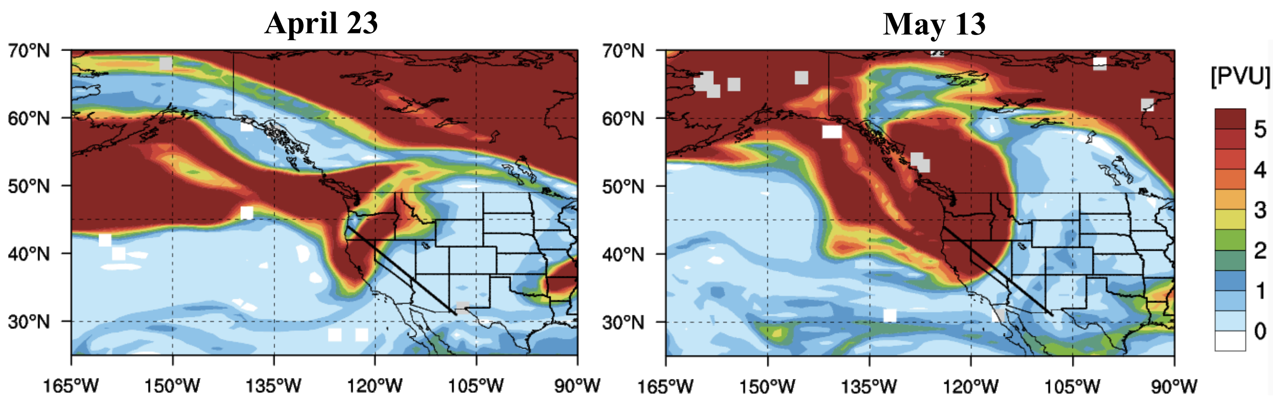

Figure S5. Potential Vorticity at 250 hPa on April 23 and May 13 (STT days), calculated from the NCEP-FNL reanalysis data.

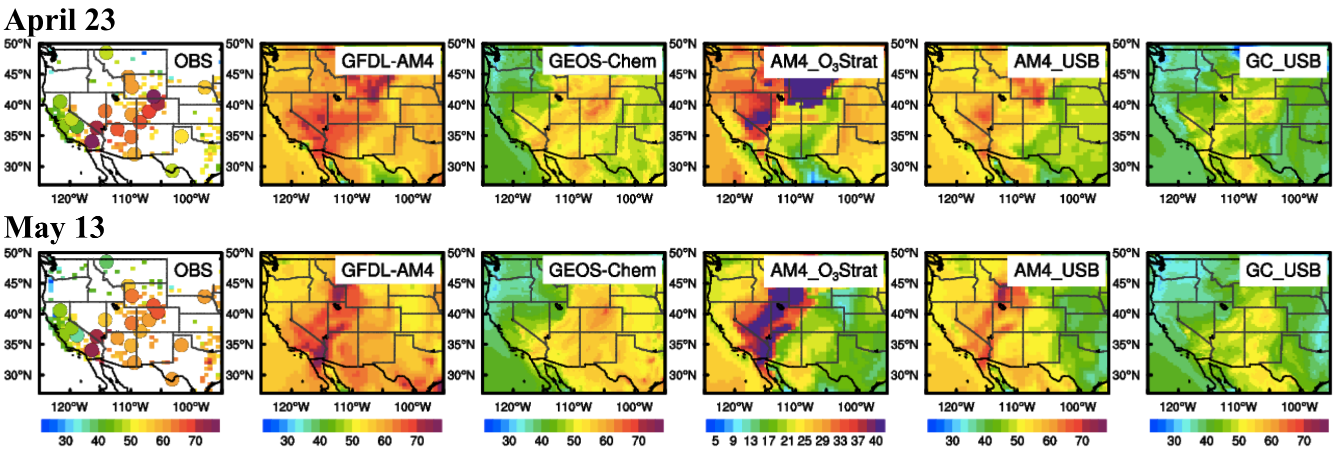

Figure S6. Maps of total MDA8 O_3 as observed and simulated with GFDL-AM4 and GEOS-Chem, along with AM4 stratospheric O_3 tracer and USB O_3 from the two models, during the STT events on April 23 and May 13, 2017.

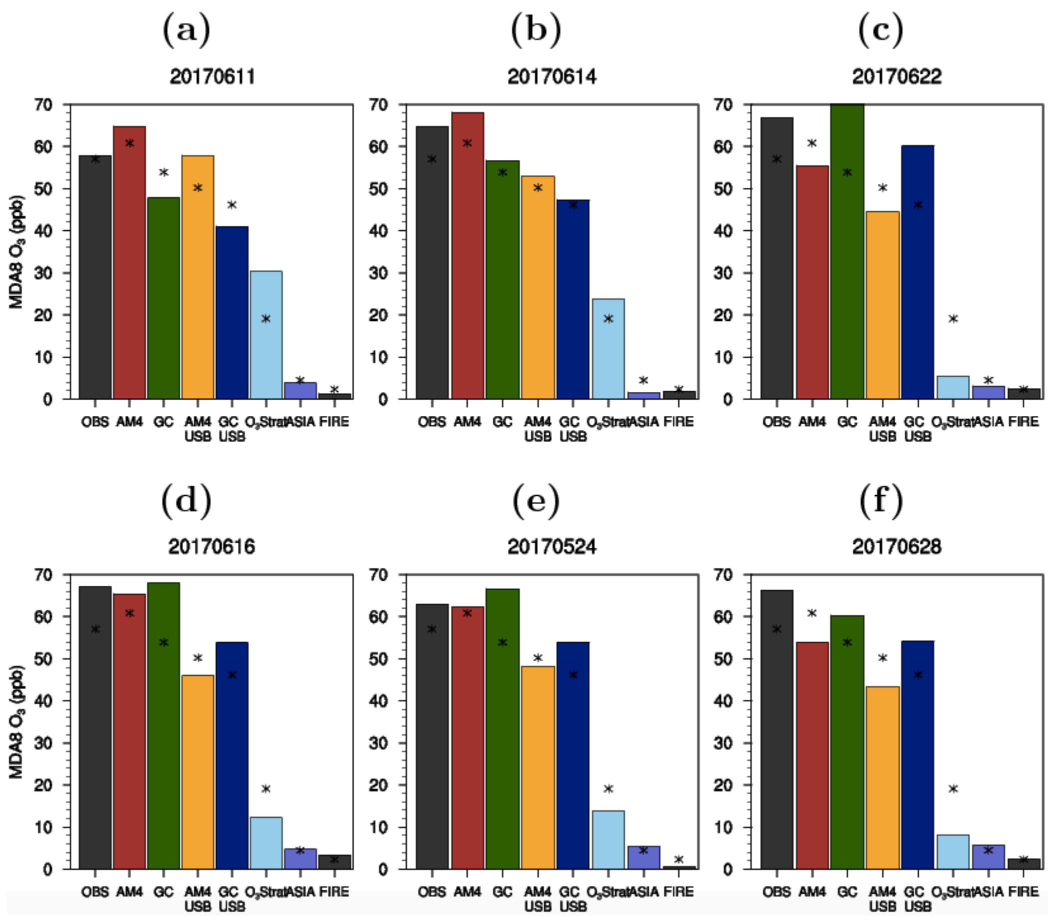

Figure S7. Statistics of MDA8 O_3 at 12 low-elevation (<1000 m altitude) air quality monitoring sites in the Las Vegas Valley as observed (OBS) and simulated with GFDL-AM4 (AM4) and GEOS-Chem (GC), along with USB O_3 from the two models, and contributions from stratospheric O_3 (O_3Strat), Asian pollution (ASIA), and wildfires (FIRE) estimated with GFDL-AM4 on (a) June 11, (b) June 14, (c) June 22, (d) June 16, (e) May 24, and (f) June 28, 2017. The star markers denote the mean values during the entire FAST-LVOS period (May-June, 2017).

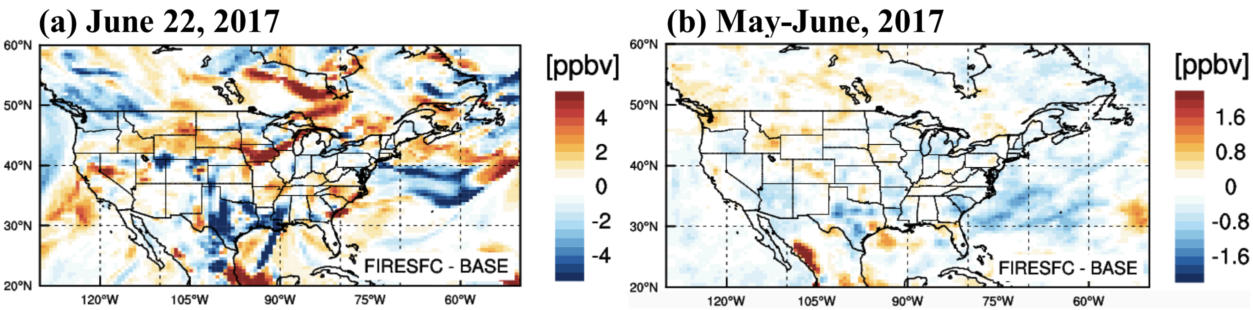

Figure S8. Differences in MDA8 O_3 between GFDL-AM4 FIRESFC (with all wildfire emissions placed at the surface) and BASE (a) on June 22, 2017 (wildfire event) and (b) during May-June, 2017 (FAST-LVOS). Simulations are at C192 (~50 km × 50 km) horizontal resolution.

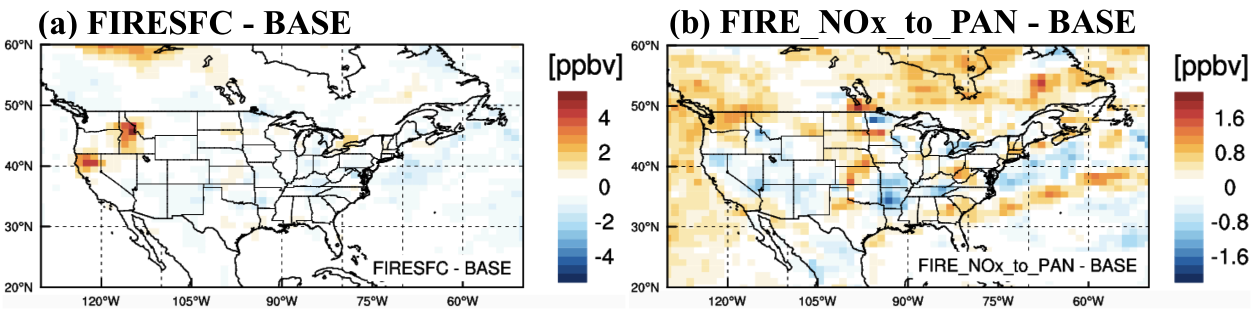

Figure S9. Monthly MDA8 O_3 differences during August, 2012 (an active wildfire season) between (a) GFDL-AM4 FIRESFC (with all wildfire emissions placed at the surface) and BASE and (b) difference between FIRE_NOx_to_PAN (with 40% and 20% of wildfire NOx partitioned into PAN and HNO_3, respectively) and BASE case. Simulations are at C96 (~100 km × 100 km) horizontal resolution. FIRE_NOx_to_PAN simulations are only available during 2010-2016.

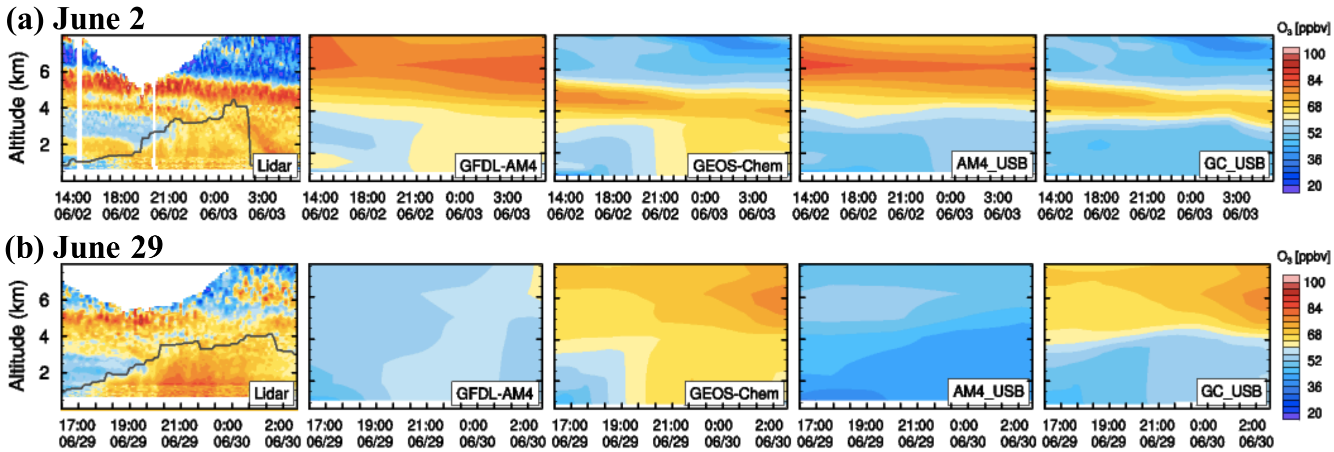

Figure S10. Time-height curtain plots of O_3 above NLVA as observed with TOPAZ lidar and simulated with GFDL-AM4 (~50×50 km^2; interpolated from 3-hourly data) and GEOS-Chem (0.25°×0.3125°; interpolated from hourly data) during the regional pollution events on (a) June 2 and (b) June 29, 2017 (UTC). The right panels compare USB O_3 from the two models.

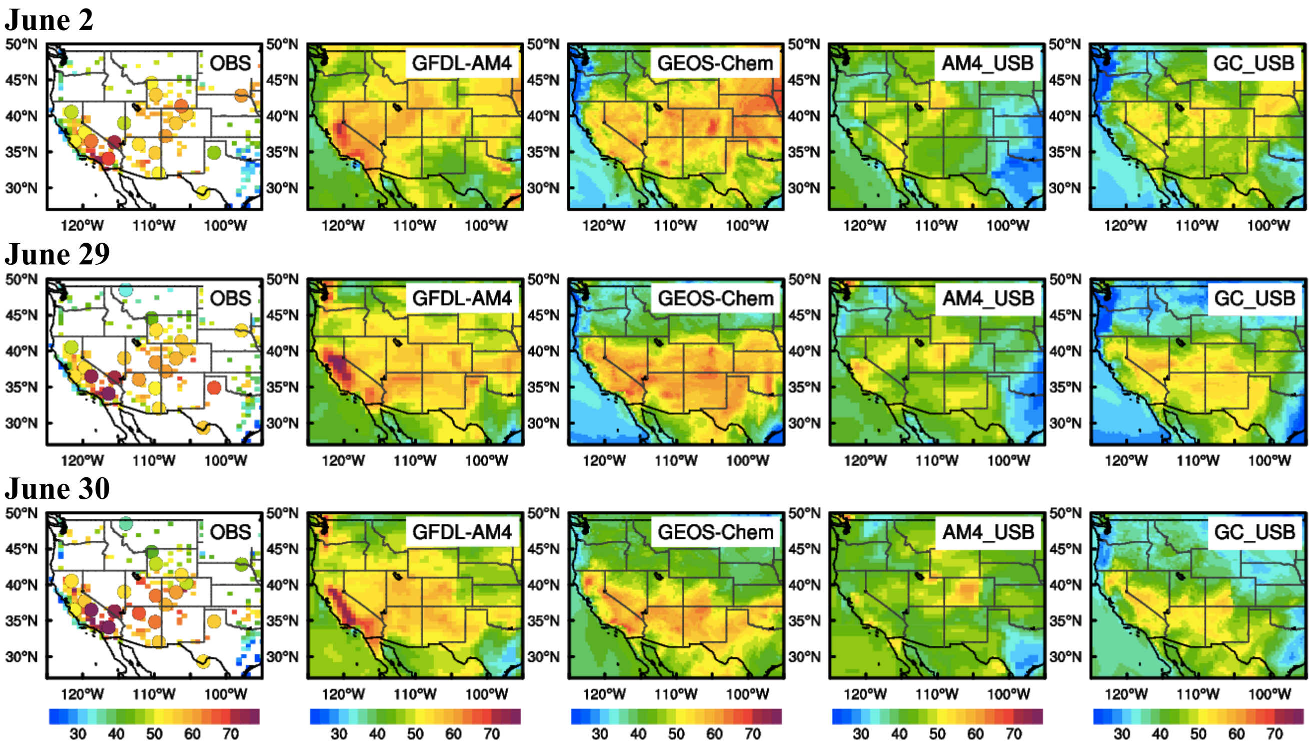

Figure S11. Same as Figure S6, but for June 2, June 29, and June 30.

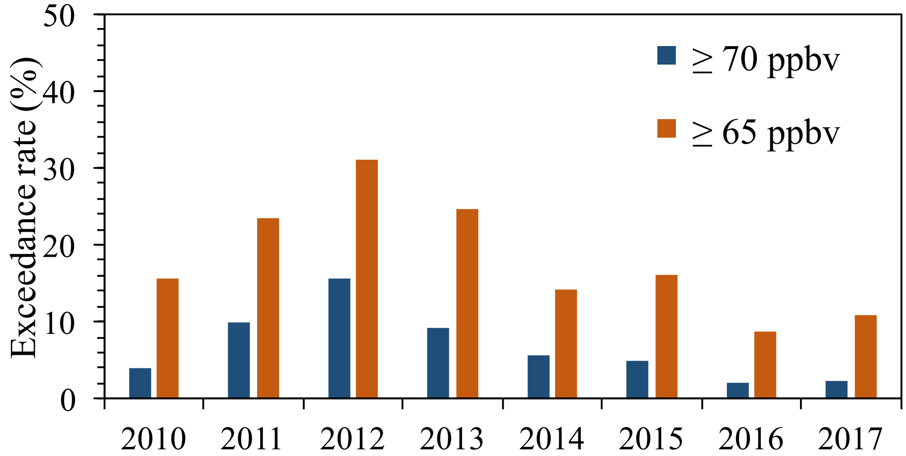

Figure S12. Rate of ozone exceedances (blue: MDA8 $O_3 \geq 70$ ppbv; red: MDA8 $O_3 \geq 65$ ppbv) at air quality monitoring sites in Clark County (% of site-days) during April-June of 2010-2017.

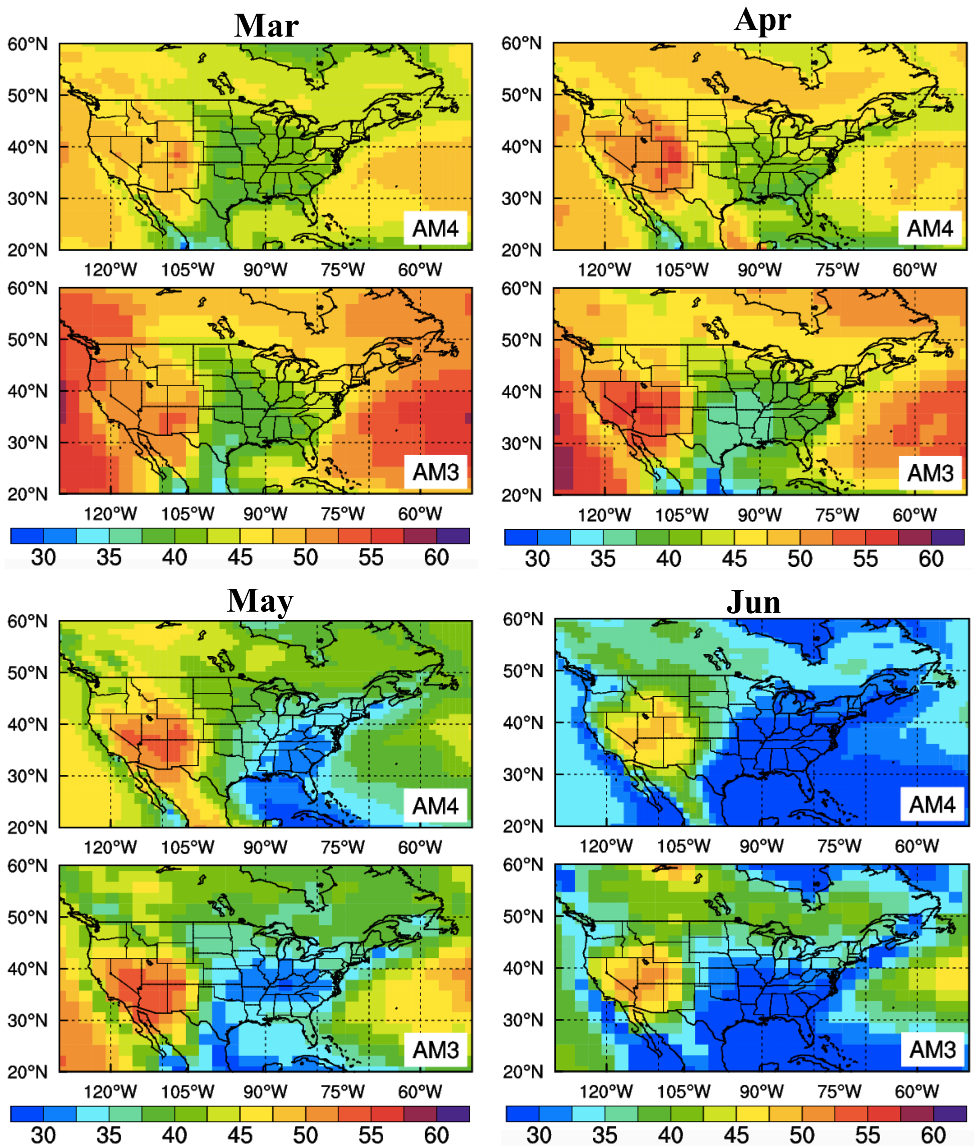

Figure S13. Comparison of NAB O_3 estimates in the GFDL-AM4 model (this study) with its predecessor GFDL-AM3 (Lin et al., 2012a; Lin et al., 2017). The results are shown separately for March to June during the 2010-2014 periods for which the NAB simulations are available from both models.

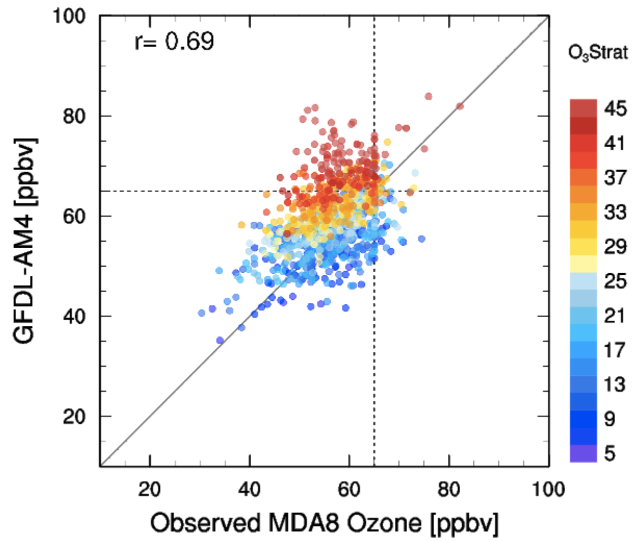

Figure S14. Scatter plots of observed versus simulated daily MDA8 O_3, color-coded by AM4 stratospheric O_3 tracer (O_3Strat) at 12 WUS high-elevation sites during April-June, 2017.

Table S1. Air quality monitoring sites in Clark County, NV and CASTNet sites in the western U.S. used in this study.

Site ID	Site Name	Latitude (º)	Longitude (º)	Elevation (m)	City/State
		Clark County sites			
32-003-0601	Boulder City	35.98	-114.85	750	Boulder City, NV
32-003-0298	Green Valley	36.05	-115.05	562	Henderson, NV
32-003-1019	Jean	35.79	-115.36	924	Jean, NV
32-003-0043	Paul Meyer	36.11	-115.25	736	Las Vegas, NV
32-003-0071	Walter Johnson	36.17	-115.26	780	Las Vegas, NV
32-003-0073	Palo Verde	36.17	-115.33	939	Las Vegas, NV
32-003-0075	Joe Neal	36.27	-115.24	732	Las Vegas, NV
32-003-0540	Jerome Mack	36.14	-115.08	549	Las Vegas, NV
32-003-0022	Apex	36.39	-114.91	661	Apex, NV
32-003-0023	Mesquite	36.81	-114.06	488	Mesquite, NV
32-003-2002	JD Smith	36.19	-115.12	569	North Las Vegas, NV
32-003-7772	Indian Springs	36.57	-115.68	977	Indian Springs, NV
32-003-0078	Arden Peak	35.95	-115.04	1311	Henderson, NV
32-003-7771	SM Youth Camp	36.32	-115.59	2569	Las Vegas, NV
		High-elevation sites (>1500 m above sea level)			
AP	Angel Peak*	36.32	-115.57	2682	Las Vegas, NV
CHA467	Chiricahua NM	32.01	-109.39	1570	AZ
PET427	Petrified Forest	34.82	-109.89	1723	AZ
GRC474	Grand Canyon NP	36.06	-112.18	2073	AZ
ROM406	Rocky Mountain NP	40.28	-105.55	2743	CO
GTH161	Gothic	38.96	-106.99	2926	CO
MEV405	Mesa Verde NP	37.20	-108.49	2165	CO
GRB411	Great Basin NP	39.01	-114.22	2060	NV
CAN407	Canyonlands NP	38.46	-109.82	1809	UT
PND165	Pinedale	42.93	-109.79	2388	WY
CNT169	Centennial	41.36	-106.24	3178	WY
YEL408	Yellowstone NP	44.56	-110.40	2400	WY

*NOAA mobile laboratory measurements

Table S2. Model configurations of GFDL-AM4 and GEOS-Chem base simulations.

Model	Horizontal resolution	Vertical resolution	Meteorological fields	U.S. Anthropogenic emissions	Biomass burning emissions	Biogenic emissions	Tropospheric chemistry	Stratospheric chemistry
GFDL-AM4	C96 (~100 km ×100 km) and C192 (~50 km×50 km) (Global)	49	Chemistry-Climate model; horizontal winds (u, v) are nudged to NCEP	Adjusted CMIP6 (NOx reduced in the EUS; see section 2.4)	FINN	MEGAN	Based on MOZART-2 (Horowitz et al., 2003; Horowitz et al., 2007)	Based on AMTRAC (Austin and Wilson, 2006; Austin et al., 2013)
GEOS-Chem	2°×2.5° (Global) and 0.25°×0.3125° (North America)	47	GEOS-FP	Adjusted NEI2011 (NOx reduced in the EUS; see section 2.4)	FINN	MEGAN	Tropchem	Linoz

Table S3. List of GFDL-AM4 and GEOS-Chem model simulations

Case	Simulation period	Emissions
GFDL-AM4		
C96_BASE	Jan 2010- Jun 2017	CMIP6 emissions but with adjusted anthropogenic NO_X emissions in China and the eastern U.S.; daily fire emissions from FINN
C96_USB	Jan 2010- Jun 2017	Same as BASE with U.S. anthropogenic emissions turned off
C96_zeroAsia	Jan 2010- Jun 2017	Same as BASE with Asian anthropogenic emissions turned off
C96_zeroFire	Jan 2010- Jun 2017	Fire emissions turned off
C192_BASE	Jan- Jun 2017	Same as C96_BASE
C192_USB	Jan- Jun 2017	Same as C96_USB
C192_zeroAsia	Jan- Jun 2017	Same as C96_zeroAsia
C192_zeroFire	Jan- Jun 2017	Same as C96_zeroFire
GEOS-Chem		
GC_Global	2017	NEI11 over U.S. and MIX in China but with adjusted anthropogenic NO_X emissions in China and the eastern U.S.; daily fire emissions from FINN
GC_NA	Apr-Jun 2017	Same as GC_Global, but only for North America
GC_USB	Apr-Jun 2017	Same as GC_NA with U.S. anthropogenic emissions turned off

Table S4. May-June mean MDA8 O_3 from observations and GFDL-AM4 simulations (C96_BASE) at 14 Clark County air quality monitoring sites from 2010 to 2017, along with model-estimated contributions from U.S. background (USB), North American Background (NAB), stratosphere-to-troposphere transport (O_3Strat), long-range transport of Asian pollution (ASIA), and wildfires (FIRE).

May-Jun	OBS	BASE	USB	NAB	O_3Strat	ASIA	FIRE
2010	58.2	63.2	52.6	48.9	20.5	4.7	2.3
2011	60.6	65.3	54.1	50.9	22.0	5.7	3.4
2012	64.3	65.7	55.3	51.6	20.4	4.2	2.7
2013	61.2	63.7	53.7	50.7	20.4	4.6	2.5
2014	59.2	61.8	51.5	47.4	18.4	4.3	1.4
2015	59.3	63.9	51.8	46.6	16.5	3.3	1.5
2016	56.4	60.7	48.9	44.3	14.9	3.8	1.8
2017	57.0	61.7	50.9	46.8	17.9	4.2	2.2
Mean±s.d.	59.5±2.5	63.2±1.8	52.3±2.0	48.4±2.6	18.9±2.4	4.4±0.7	2.2±0.7

References

Austin, J., and Wilson, R. J.: Ensemble simulations of the decline and recovery of stratospheric ozone, J. Geophys. Res.-Atmos., 111, https://doi.org/10.1029/2005JD006907, 2006.

Austin, J., Horowitz, L. W., Schwarzkopf, M. D., Wilson, R. J., and Levy II, H.: Stratospheric Ozone and Temperature Simulated from the Preindustrial Era to the Present Day, J. Climate, 26, 3528-3543, https://doi.org/10.1175/jcli-d-12-00162.1, 2013.

Horowitz, L. W., Walters, S., Mauzerall, D. L., Emmons, L. K., Rasch, P. J., Granier, C., Tie, X., Lamarque, J.-F., Schultz, M. G., Tyndall, G. S., Orlando, J. J., and Brasseur, G. P.: A global simulation of tropospheric ozone and related tracers: Description and evaluation of MOZART, version 2, J. Geophys. Res.-Atmos., 108, https://doi.org/10.1029/2002JD002853, 2003.

Horowitz, L. W., Fiore, A. M., Milly, G. P., Cohen, R. C., Perring, A., Wooldridge, P. J., Hess, P. G., Emmons, L. K., and Lamarque, J.-F.: Observational constraints on the chemistry of isoprene nitrates over the eastern United States, J. Geophys. Res.-Atmos., 112, https://doi.org/10.1029/2006JD007747, 2007.